Reaction Kinetics, Mechanisms and Catalysis (2020) 131:691–706
https://doi.org/10.1007/s11144-020-01870-0

Cu/CeO_2 as efficient low-temperature CO oxidation catalysts: effects of morphological structure and Cu content

Chunlei Wu[1] · Zengzeng Guo[1] · Xiaoyu Chen[1] · Hong Liu[1]

Received: 7 July 2020 / Accepted: 16 September 2020 / Published online: 19 September 2020

Abstract

Cu loaded on different morphologies of CeO_2 were synthesized and tested by SEM and CO catalytic oxidation experiment, the results indicated that with the same Cu load, nanorod-like Cu/CeO_2 performed the best catalytic activity than 3D flower-like Cu/CeO_2 and gear-like Cu/CeO_2. Then nanorod-like Cu/CeO_2 were chose to explore the best Cu load on CeO_2 nanorods for CO oxidation. Cu/CeO_2 nanorods were characterized by TEM, XRD, XPS as well as physical and chemical adsorption. The results indicate that $0.15Cu/CeO_2$ nanorods have the best catalytic activity because of more reducing copper species (Cu^+), adsorbed oxygen (O_{ads}) and Ce^{3+} species on the catalysts surface, which can achieve 99% CO conversion at 100 °C. The effect of CO_2 and water vapor on catalytic activity was also examined.

Keywords Cu/CeO_2 nanorods · Morphology · CO catalytic oxidation · Low temperature oxidation · Optimal load

Introduction

Air pollution caused by automobile exhaust, waste gas of coal mines and incomplete combustion of hydrocarbons becomes increasingly serious nowadays [1]. The air pollutants include SO_2, NO_x, CO and suspended particulate matter. Among these, CO is the most dangerous one because its affinity with hemoglobin is over 200 times than oxygen [2], thus easily causes human death. Hence, the elimination of CO is of great significance for protecting the environment and human health.

Electronic supplementary material The online version of this article (https://doi.org/10.1007/s11144-020-01870-0) contains supplementary material, which is available to authorized users.

✉ Xiaoyu Chen
drizzle13xy@126.com

[1] Jiangsu Key Laboratory of Fire Safety in Urban Underground Space, China University of Mining and Technology, Xuzhou 221116, Jiangsu, People's Republic of China

Recently, catalytic oxidation method is widely employed for CO elimination due to its high conversion and environmentally friendliness. Catalysts commonly used for CO catalytic oxidation include noble metal catalysts and non-noble metal catalysts [3, 4]. Although noble metal catalysts have good catalytic performance, the disadvantages of their high cost, high sintering temperature and low poison tolerance restrain their application [5, 6]. Non-noble metal catalysts have become promising catalysts because of their low cost and potential applications in various fields. Among non-noble metal catalysts, CeO_2 has attracted much attention due to its excellent oxygen storage capacity (OSC), inherent Ce^{3+}/Ce^{4+} redox electron pair and rich oxygen vacancy [7–9]. Although a large amount of research has been devoted to the preparation of cerium-based catalysts, a challenging problem which arises is that CO cannot be completely oxidized unless at relatively high temperatures.

A series of transition metal oxides have been introduced to the cerium-based catalysts to improve their CO catalytic performance at low temperature [10–12]. Doping CeO_2 with transition metals could generate oxygen vacancies or surface defects in the ceria lattice, which are essential to CO oxidation [13, 14]. Lykaki et al. [13] reported the effect of ceria nanoparticles shape and Cu doped ceria on CO oxidation. They found that Cu/CeO_2 nanorods had an excellent catalytic performance of complete CO conversion at 150 °C compared with Cu/CeO_2 nanopolyhedra and Cu/CeO_2 nanocubes. Besides, Mn-CeO_2, Co-CeO_2 and Ni-CeO_2 nanorods also show high catalytic activity compared with pure CeO_2 nanorods [14]. These results indicate transition metal doped ceria catalysts exhibit higher CO oxidation activity compared with pristine CeO_2 nanorods, but Cu doped ceria catalysts show the best catalytic effect for CO oxidation.

In this work, Cu loaded on nanorod-like, 3D flower-like and gear-like CeO_2 were synthesized and the CO catalytic performance were tested. Nanorod-like CeO_2 with excellent CO catalytic performance was applied to investigating the effects of Cu load, and different ratios of Cu was loaded on CeO_2 nanorods with different ratios by wet impregnation method [13, 15]. We report syntheses, surface structure, chemisorption property, and CO catalytic activity (including the influence of water and CO_2) of a serious of Cu/CeO_2 nanorods and have found an optimal Cu load to CeO_2. Our results indicate that the morphology CeO_2 and Cu load play vital role in CO catalytic performance. From a micro point of view, structural defects and active sites dominate the surface catalyst reaction of copper-ceria binary oxides.

Experimental

Synthesis of CeO_2 and Cu/CeO_2 nanorods

Synthesis of nanorod-like CeO_2

All chemicals were commercially purchased and used without further purification. CeO_2 nanorods were synthesized by a hydrothermal method following the reported procedures [16], with minor modifications. $Ce(NO_3)_3{\cdot}6H_2O$ (4.5 mmol) was dissolved in aqueous KOH solution (90 mL, 6 M) in a Teflon bottle and stirred at room

temperature for 30 min, then the mixture was transferred into a stainless-steel autoclave, sealed tightly and maintained at 100 °C for 12 h. After cooling to room temperature, the precipitate obtained was collected by filtration and washed with deionized (DI) water. The final precipitate was dried in vacuum at 80 °C for 4 h and calcined at 400 °C in air for 4 h (heating ramp 3 °C/min).

Synthesis of 3D flower-like CeO_2

3D flower-like CeO_2 was synthesized by the reported procedures [17]. 1.5 g $CeCl_3{\cdot}6H_2O$, 2.2 g urea and 6 g tetrabutylammonium bromide (TBAB) were added to 150 mL ethylene glycol in a 250-mL round flask. The obtained solution was stirred with a magnetic stir bar and was heated to 180 °C. 30 min later, the reaction was stopped and the mixture was cooled to room temperature. The precipitate as ceria precursor was collected by centrifugation and washed with ethanol for 4 times. Ceria was from the as-prepared precursor via calcinations in air at 450 °C for 2 h (heating ramp 3 °C/min).

Synthesis of gear-like CeO_2

Gear-like CeO_2 was synthesized by the reported procedures [18]. 4 mmol cetyltrimethyl ammonium bromide (CTAB) and 40 mmol NH_4HCO_3 were dissolved in 20 mL distilled water under vigorous stirring for 30 min. 8 mmol $Ce(NO_3)_3{\cdot}6H_2O$ were dissolved in 20 mL distilled water under vigorous stirring for 30 min. Then 20 mL $Ce(NO_3)_3{\cdot}6H_2O$ aqueous solution were added to 20 mL CTAB and NH_4HCO_3 aqueous solution under continuous stirring for 30 min, forming a homogeneous solution. The mixed solution was transferred into a 50 mL Teflon-lined autoclave and heated at 180 °C for 12 h. After the autoclave was cooled to room temperature naturally, fresh precipitates were washed with distilled water and ethanol for three times, and then dried at 80 °C overnight. CeO_2 microstructures were obtained by calcinating at 400 °C for 5 h (heating ramp 3 °C/min), accompanied by a color change from white to slight yellow.

Synthesis of Cu/CeO_2 catalysts

Cu/CeO_2 catalysts were synthesized by wet impregnation method, using an aqueous solution of $Cu(NO_3)_2{\cdot}3H_2O$ to obtain different Cu/(Cu + Ce) atomic ratios of 0.05, 0.1, 0.15 and 0.2. The suspensions were heated under stirring to remove excess water. Finally, the obtained precipitate was dried at 80 °C for 4 h and calcined at 400 °C in air for 4 h (heating ramp 3 °C/min). The obtained catalysts were denoted as xCu/CeO_2, in which x represented Cu/(Cu + Ce) atomic ratios.

Catalysts characterization

SEM, TEM and HRTEM analysis

The scanning electron microscope (SEM) images were collected by HITACHI SU8010 scanning electron microscope. Transmission electron microscopy (TEM) and high-resolution transmission electron microscopy (HRTEM) characterizations was examined by using a TECNAI G2 F20 instrument operated at 100 kV. 400 mesh copper grid covered by ultrathin carbon film (Ted Pella) was used. To prepare the TEM samples, the catalyst powder samples were first dispersed in ethanol and then sonicated for 30 min. One or two drops of the sample suspension from the sonicated solution using a small pipette were poured on the copper grid.

Textural characterization

The measurement of the surface area (S_{BET}), average pore size and total pore volume of the catalysts were operated on a Quantachrome autosorb iQ ASIQMU0001000-7 with N_2 adsorption isotherms at − 196 °C. The surface area (S_{BET}) was calculated using the Brunauer–Emmett–Teller (BET) method, the pore size distribution curves were determined from the adsorption branches calculated by the Barrett-Joyner-Halenda (BJH) method and the total pore volume was calculated based on the adsorbed nitrogen at the relative pressure of 0.995. Prior to the measurements, the samples were degassed at 300 °C for 3 h.

X-ray diffraction

The crystalline structure of the catalysts was performed by a Bruker D8 Advance X-ray diffractometer equipped with Cu K_α radiation ($\lambda = 0.154$ nm), which with accelerating voltage of 40 kV and emission current 40 mA. The scan range (2θ) is between 10 and 80° with a scan rate of 1° min^{-1}. JADE software was used to calculate the average crystallite size using the Scherrer equation.

XPS studies

The surface composition and chemical valence state of the samples was analyzed by X-ray photoelectron spectroscopy (XPS) using a Thermo Scientific, Escalab 250Xi spectrometer, and the energy calibration was performed using contaminated carbon (C 1 s, BE = 284.8 eV) as standard.

TPR and TPD analysis

Temperature programmed reduction (TPR) experiments were performed by using Micromeritics Autochem™ II 2920 chemisorption analyzer to determine the reduction temperature and amount of hydrogen consumption. The samples (50 mg) were reduced with a mixture of 1.53 V% H_2/Ar (30 mL/min) and the temperature was increased from ambient temperature to 800 °C at the rate of 10 °C/min. Prior to

the TPR experiment, the sample was treated by heating from ambient temperature to 150 °C for 30 min under pure argon flow, in order to clean the sample surface. The consumption of H_2 was detected by a TCD detector. CO-TPD measurement was conducted at the same instrument as H_2-TPR. The sample was pretreated under He flow at 150 °C for 30 min. After cooling to room temperature in He flow, 5%CO/He gas was flown at 50 mL/min through the sample for 30 min. The sample was reheated up to 450 °C at 10 °C/min under He gas and the desorption behavior of CO can be analyzed at elevated temperature.

Catalytic activity measurements

The catalytic evaluation was performed in a quartz fixed-bed reactor with 10 mm internal diameter, loaded with 200 mg of catalyst. The reactant gas composed of 3 V% gaseous CO balanced with 15 V% O_2 in N_2 was flowed into the reactor at a flow rate of 100 cm^3/min. Catalytic evaluation measurements were carried out by increasing the temperature by 10-degree steps from 30 °C up to 150 °C. The catalyzed gas were measured by an online gas chromatography. The CO catalytic activity was evaluated by using the following equations:

$$X_{CO}(\%) = \frac{CO_{inlet} - CO_{outlet}}{CO_{inlet}} \times 100\%$$

Here X_{CO}, CO_{inlet} and CO_{outlet} are the conversion of CO, CO concentration (ppm) in the inlet and outlet gas streams.

Results and discussion

CO oxidation

Fig. 1 shows the CO catalytic performance of nanorod-like 0.10Cu/CeO_2, 3D flower-like 0.10Cu/CeO_2 and gear-like 0.10Cu/CeO_2. Nanorod-like 0.10Cu/CeO_2 performs the best catalytic activity with a 90% CO catalytic conversion at 96 °C. While for 3D flower-like 0.10Cu/CeO_2 and gear-like 0.10Cu/CeO_2, the temperatures required to achieve 90% CO catalytic conversion are 139 °C and 135 °C. The possible reasons of the catalytic differences will be described in SEM below. In view of the excellent catalytic performance of the nanorod-like Cu/CeO_2 catalyst, we choose the nanorod-like Cu/CeO_2 catalyst to explore the influence of different copper loading on the CO catalytic performance, and the influence of CO_2 and water on the catalytic performance of the catalyst are also explored.

Fig. 2 displays the catalytic activity of CO oxidation over CeO_2 and Cu/CeO_2 nanorods. The conversion curves of CO show S-shaped growth with the increase of temperature. Pure CeO_2 nanorods perform a poor CO catalytic activity, they can achieve a complete CO conversion until 350 °C. The addition of copper to the CeO_2 nanorods greatly improves the catalytic efficiency. CO catalytic conversion does not increase monotonously with the copper loading, instead there is an optimal

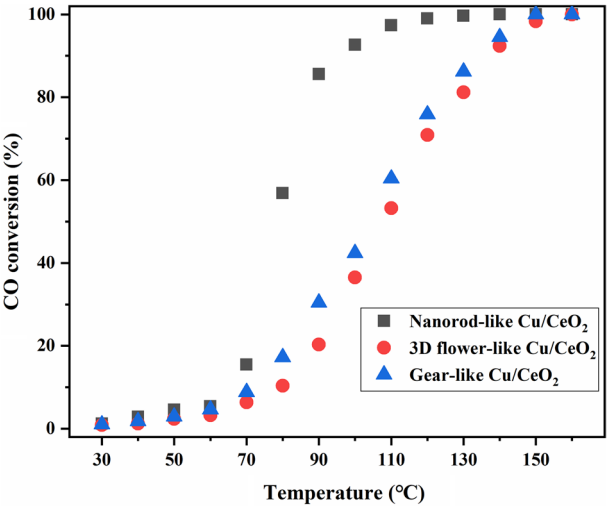

Fig. 1 CO conversion as a function of temperature for nanorod-like 0.10 Cu/CeO_2, 3D flower-like $0.10Cu/CeO_2$ and gear-like $0.10Cu/CeO_2$ ($CO/O_2/N_2 = 3/15/82$, the flow rate is 100 cm^3/min, $m_{cat} = 0.2$ g)

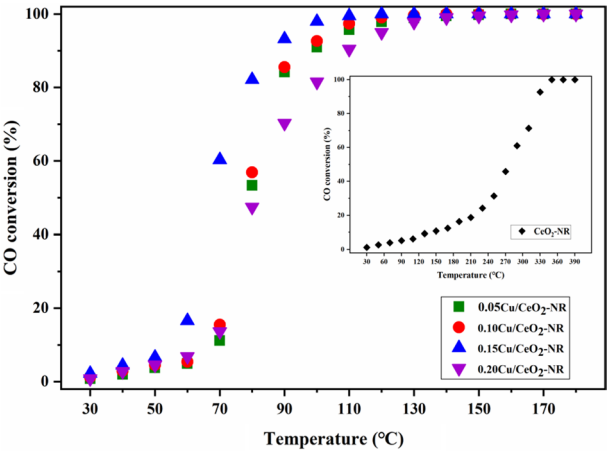

Fig. 2 CO conversion as a function of temperature for CeO_2 and Cu/CeO_2 nanorods ($CO/O_2/N_2 = 3/15/82$, the flow rate is 100 cm^3/min, $m_{cat} = 0.2$ g)

copper loading. Before reaching the optimal copper loading, the catalytic efficiency increases gradually with copper loading. While when the copper loading exceeds the optimal copper loading, the catalytic efficiency begins to decrease. The possible reason is that when the copper loading exceeds the optimum value, agglomeration will occur on the nanorods surface. Agglomeration of the nanorods will lead to the enlargement of the nanorods, the coverage of the active sites of copper and the reduction of oxygen vacancies, thus reducing the catalytic efficiency, as will be

discussed below. As shown in Fig. 2, 0.15Cu/CeO_2 nanorods performs the best catalytic activity with a 50% CO catalytic conversion at 68 °C and a 90% CO catalytic conversion at 87 °C. Besides, when the temperature is higher than 100 °C, the catalytic CO conversion is greater than 99%. The conversions of CO over these nanorods are in the following order: 0.15Cu/CeO_2 > 0.10Cu/CeO_2 > 0.05Cu/CeO_2 > 0.20Cu/CeO_2 > CeO_2, and the complete CO conversion is achieved at 120 °C, 140 °C, 150 °C, 170 °C, 350 °C.

In order to investigate the effect of CO_2 and water vapor on nanorods, water and CO_2 were added to the reaction gas to test the catalytic efficiency of 0.15Cu/CeO_2 nanorods. As displayed in Fig. 3, when 5 V% CO_2 was introduced, CO_2 inhibit the CO oxidation due to the competitive adsorption between CO and CO_2 on copper sites, but the temperature required for complete conversion of the nanorods was almost unchanged. However, when 9.4 V% H_2O was injected into the reaction gas, the catalytic activity was greatly affected and the complete conversion has reached to 160 °C. When 5 V% CO_2 and 9.4 V% H_2O were added to the reaction gas at the same time, the catalytic efficiency further decreased, and CO could be completely oxidized at 190 °C. The main reason why water reduces the catalytic activity is that water molecules will be adsorbed on the active sites, affecting CO adsorption on the surface of nanorods. Therefore, a conclusion can be drawn that CO_2 has less influence while water has greater influence on the catalytic efficiency of the nanorods.

Morphological characterization (SEM and TEM)

The SEM images of CeO_2 samples with different morphological characterization are shown in Fig. S1. The nanorod-like morphology of CeO_2, and many nanorod-like CeO_2 precursors form sheet-like structures (Fig. S1a). 3D flowerlike micro/

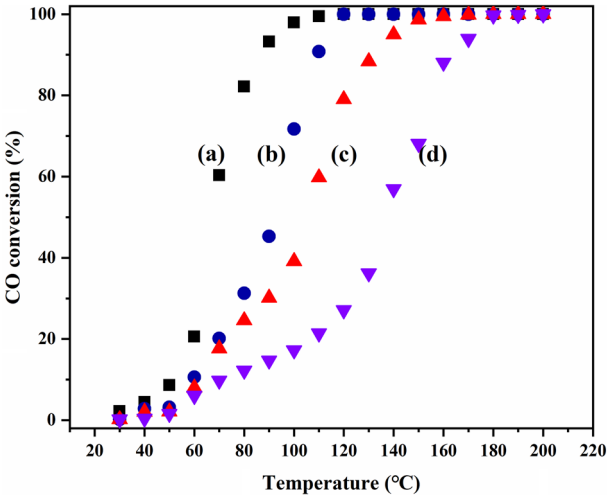

Fig. 3 Effect of 5 V% CO_2 and 9.4 V% H_2O on CO conversion (a) in the absence of CO_2 and H_2O, (b) in the presence of 5 V% CO_2, (c) in the presence of 9.4 V% H_2O, (d) in the presence of 5 V% CO_2 and 9.4 V% H_2O (CO = 3%, O_2 = 15%, the flow rate is 100 cm^3/min, m_{cat} = 0.2 g)

nanostructure can be seen from Fig. S1b, the SEM image indicates the entire structure of the architecture was built from micropetals which connected with each other forming the cured 3D flowerlike micro/nanostructure by self-assembly. Fig. S1c shows the gear-like microstructures of 1 mm in diameter. From the comparison of the above three morphological characterizations, the nanorod-like CeO_2 has smaller size. And due to CeO_2 nanorods have larger specific surface areas than other morphological characterization of CeO_2 and preferentially expose certain specific crystal planes with high catalytic activity, thus exhibiting higher CO catalytic activity [19].

In order to further understand the structural characteristics of nanorod-like CeO_2, the morphological characterization of pure CeO_2 and 0.15Cu/CeO_2 nanorods were investigated by transmission electron microscopy (TEM). The pure CeO_2 nanorods show rod-like morphology with the diameter of 7.6 nm and length of 30–60 nm (Fig. 4a). When copper is doped on CeO_2 nanorods, the diameter of the nanorods were reduced to 7.1 nm (Fig. 4c), which may increase the specific surface areas of the nanorods. Fig. 5b and d show the HRTEM images of the nanorods. The lattice fringes are clearly visible with the spacings of 0.311, 0.271, 0.194 nm (Fig. 4b),

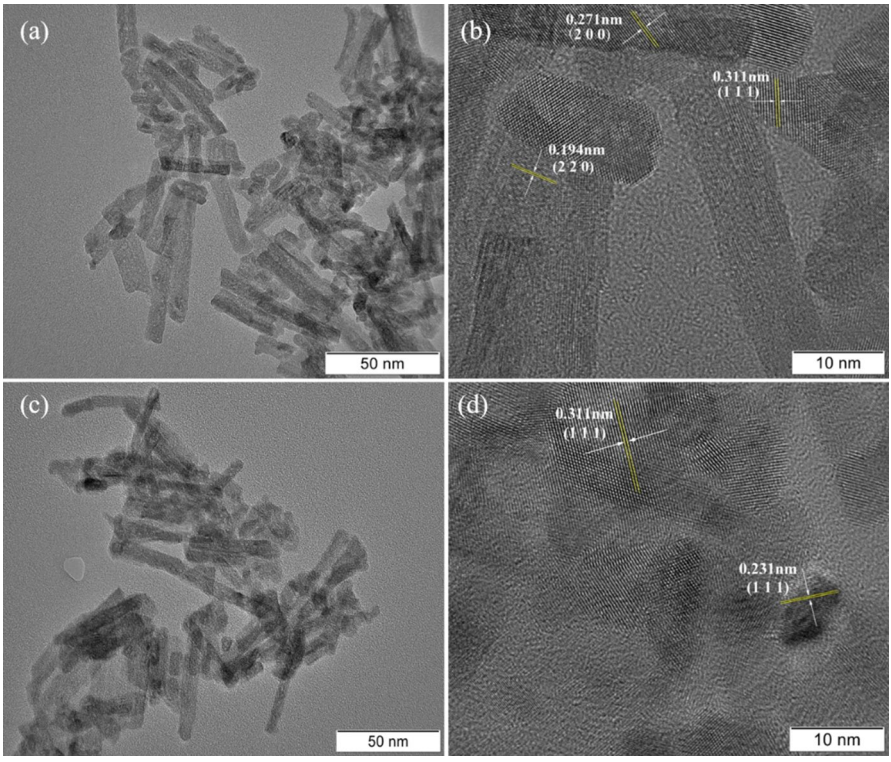

Fig. 4 TEM images of the obtained nanorods **a** TEM image of the pure CeO_2 nanorods, **b** HRTEM image of the pure CeO_2 nanorods, **c** TEM image of the 0.15Cu/CeO_2 nanorods, **d** HRTEM image of the 0.15Cu/CeO_2 nanorods

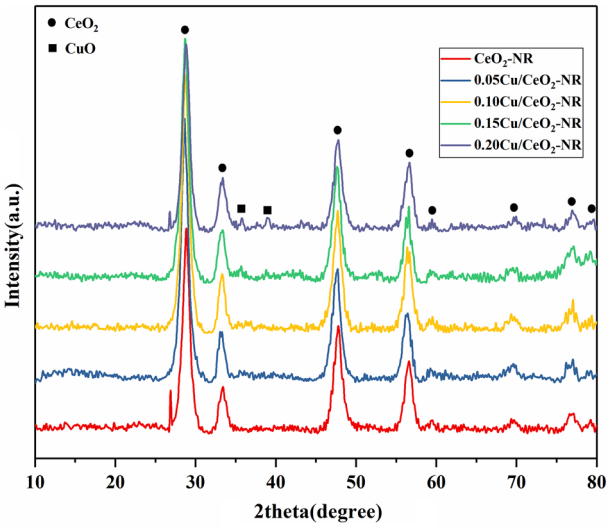

Fig. 5 XRD patterns of the obtained CeO_2 and Cu/CeO_2 nanorods

corresponding to the (111), (200) and (220) crystalline planes of CeO_2 nanorods [20]. The lattice fringes with distances of 0.311 nm and 0.231 nm (Fig. 4d) are in good agreement with the (111) plane of CeO_2 and (111) plane of CuO [21].

Crystal structures, sizes, and surface areas

The crystal structure of the obtained CeO_2 and Cu/CeO_2 nanorods is determined by XRD (Fig. 5). The main XRD peaks of all the Cu doped CeO_2 samples centered at $2\theta = 28.8°$, 33.4°, 47.9°, 56.9°, 59.7°, 69.7°, 77.0° and 79.2°, which can be indexed to (111), (200), (220), (311), (222), (400), (331) and (420) planes of pure fluorite type cubic CeO_2 (JCPDS 43-1002) [22], indicating that the Cu doping does not change their crystal structure. In addition, two diffraction peaks for CuO with a monoclinic structure were observed at $2\theta = 35.8°$ and 39.0°, which correspond to (-111) and (111) planes (JCPDS 45-0937) [23], respectively, suggesting that the formation of bulk CuO on the surface of CeO_2. The average crystallite diameter of CeO_2 phases calculated by the Scherrer equation is also summarized in Table 1. The diameters of CeO_2 for the pristine CeO_2 and Cu/CeO_2 nanorods are in the range of 6.9–8.8 nm, among them, the $0.15Cu/CeO_2$ nanorod has the smallest crystal size. It is also found that when Cu/(Cu + Ce) atomic ratios increase from 0.05 to 0.15, the crystallite sizes of CeO_2 decrease gradually, but when Cu/(Cu + Ce) atomic ratios increase to 0.20, the crystallite sizes of CeO_2 begin to increase, indicating that the addition of appropriate Cu species can reduce the sizes of crystallite.

The obtained CeO_2 and Cu/CeO_2 nanorods are characterized by the N_2 adsorption and desorption profiles (Table 1). The BET surface area of the undoped CeO_2 nanorods was measured to be 102.6 m^2/g, while the surface area increased slightly upon Cu doping except $0.20Cu/CeO_2$ nanorods. And the $0.15Cu/CeO_2$ nanorods

Table 1 Physicochemical properties of CeO_2 and Cu/CeO_2 samples

Sample	BET analysis			XRD analysis
	BET surface area (m^2/g)[a]	Average pore size (nm)[b]	Pore volume (cm^3/g)[c]	D_{XRD} (nm)[d]
CeO_2	102.6	3.855	0.309	8.6
$0.05Cu/CeO_2$	112.0	3.886	0.339	8.8
$0.10Cu/CeO_2$	116.1	3.882	0.346	7.4
$0.15Cu/CeO_2$	120.9	3.885	0.358	6.9
$0.20Cu/CeO_2$	92.2	3.863	0.278	7.5

[a]BET specific surface

[b]The average pore size calculated from the desorption branch of the isotherm using the BJH method

[c]The total pore volume measured at $P/P_0 = 0.995$

[d]The crystal sizes of CeO_2 calculated by using the Scherrer equation

present the highest BET surface area of 120.9 m^2/g. Interestingly, when Cu/(Cu + Ce) atomic ratios increase from 0.05 to 0.15, the BET surface area of CeO_2 phases follows the reverse order of average crystallite diameter, implying that the addition of appropriate copper species will increase the dispersion of CeO_2 crystallite and reduce the agglomeration of CeO_2 crystallite. The same trend was also observed by Lykaki et al. [13] and Zabilskiy et al. [24] for Cu/CeO_2 catalysts.

Surface analysis (XPS)

Fig. S2A shows the Ce 3d XPS spectra of the obtained CeO_2 and Cu/CeO_2 nanorods, which can be composed of eight components associated with the four pairs of Ce3d spin–orbit doublets. The peaks labeled as v (v–v‴) and the others marked as u (u–u‴) correspond to the $3d_{5/2}$ and $3d_{3/2}$ spin–orbit components, respectively. The main peaks at 882.0 eV (v), 888.6 eV (v″), 897.9 eV (v‴), 900.4 eV (u), 907.5 eV (u″) and 916.4 eV (u‴) are ascribed to Ce^{4+}, and the rest of two peaks at 884.4 eV (v′) and 902.8 eV (u′) are characteristics of the Ce^{3+} [25, 26]. It was reported that the presence of Ce^{3+} is beneficial to the formation of oxygen vacancy defects, and the high ratio of $Ce^{3+}/(Ce^{4+} + Ce^{3+})$ can accelerate the oxygen migration rate, thus improving the catalytic activity of the catalyst [26, 27]. The fraction of Ce^{3+} and the concentration of oxygen vacancy of the obtained nanorods have been calculated, which are shown in Table 2. The order of the surface Ce^{3+} content and the concentration of oxygen vacancy about the obtained samples perform the same trend: $0.15Cu/CeO_2 > 0.10Cu/CeO_2 > 0.05Cu/CeO_2 > 0.20Cu/CeO_2 > CeO_2$, which is perfectly matched to the order of their CO catalytic performance, indicating that Ce^{3+} species and oxygen vacancy are very likely to be related to catalysis of CO.

Fig. S2(B) shows the Cu 2p XPS spectra of Cu/CeO_2 nanorods in which the component centers at binding energy corresponds to Cu 2p3/2, and the component centers at binding energy corresponds to Cu 2p1/2. The shake-up satellite between 937.7 and 946.7 eV is the signal of the existence of Cu^{2+} ions. The components of Cu 2p3/2 and Cu 2p1/2 can be decomposed into two peaks at

Table 2 XPS results of CeO_2 and Cu/CeO_2 samples

Sample	O_{ads} (%)	O_{latt} (%)	O_{ads}/O_{latt}	Ce^{3+} (%)	V_0 (%)[a]	Cu^+ (%)	Cu^{2+} (%)	Cu^+/Cu^{2+}	I_{sat}/I_{mp}[b]
CeO_2	34.23	65.77	0.520	25.75	6.44	–	–	–	–
0.05Cu/CeO_2	38.83	61.17	0.635	28.15	7.04	63.58	36.42	1.746	0.267
0.10Cu/CeO_2	40.00	60.00	0.667	28.93	7.23	64.02	35.98	1.779	0.262
0.15Cu/CeO_2	44.01	55.99	0.786	29.42	7.36	66.40	33.60	1.976	0.249
0.20Cu/CeO_2	37.72	62.28	0.606	27.47	6.87	59.32	40.68	1.458	0.308

[a]V_0 (concentration of oxygen vacancy) was calculated by using the following formula: $[V_0] = 1 - (3[Ce^{3+}] + 4[Ce^{4+}])/4$

[b]I_{sat}/I_{mp} was calculated by the ratio of the intensity of shake-up satellite peak to the intensity of the main Cu $2p_{3/2}$ peak

932.1 eV and 933.9 eV, 951.8 eV and 953.7 eV. The peaks centered at 932.1 eV and 951.8 eV could be assigned to Cu^+, while the peaks centered at 933.9 eV and 953.7 eV are the characteristics of Cu^{2+}, indicating that the coexistence of two copper species of the Cu/CeO_2 nanorods. The existence of reduced species can be further confirmed by the intensity of the shake-up satellite contribution at high binding energy together with the intensity of the main Cu 2p3/2 peak (denoted as I_{sat}/I_{mp}). The I_{sat}/I_{mp} ratios of Cu/CeO_2 nanorods are shown in Table 2, all the I_{sat}/I_{mp} values of them are lower than 0.55, indicating that the presence of reduced copper (Cu^+) in Cu/CeO_2 nanorods [28, 29]. The following order in terms of I_{sat}/I_{mp} values of them is as follows: $0.15Cu/CeO_2 < 0.10Cu/CeO_2 < 0.05Cu/CeO_2 < 0.20Cu/CeO_2 < CeO_2$, and the Cu^+/Cu^{2+} values follows the reverse order, which is perfectly consistent with their CO catalytic activity. Furthermore, it can be also inferred that the more reducing copper species (Cu^+) are, the higher the activity of the catalyst is. And a copper-ceria interaction of $Ce^{3+} + Cu^{2+} \leftrightarrow Ce^{4+} + Cu^+$ probably happens on the surface of the Cu/CeO2 nanorods [13, 30].

Fig. S2(C) depicts the O 1s XPS spectra of the CeO_2 and Cu/CeO_2 nanorods, where two peaks (O_{latt} and O_{ads}) are clearly resolved. The low binding energy peak (denoted as O_{latt}) at 529–530 eV is the characteristics of the lattice oxygen (O^{2-}) and the high binding energy of 531–533 eV might be attributed to low coordination surface oxygen species, surface oxygen defects, as well as the surface adsorption of oxygen ions (denoted as O_{ads}) [31, 32]. The relative amount of O_{latt} and O_{ads} species are presented in Table 2. It is obvious that Cu/CeO_2 nanorods have a higher concentration of O_{ads} species in the range of 37.72–44.01% compared to pure CeO_2 (34.23%). And the $0.15Cu/CeO_2$ nanorods perform the highest population of O_{ads} species. It was reported that O_{ads} species are more active and significant for the CO catalytic activity [15]. Hence, we calculated their relative ratios to the surface lattice oxygen which were shown in Table 2. The corresponding order is as follows: 0.15Cu/CeO2 (0.786) > 0.10Cu/CeO2 (0.667) > $0.05Cu/CeO_2$ (0.635) > 0.20Cu/

CeO_2 (0.606) > CeO2 (0.520), which is in great agreement with their CO catalytic activity, suggesting that adsorbed oxygen performs the key role on CO catalysis.

H_2-TPR

H_2-TPR was carried out to determine the amount of H_2 consumption and reduction temperature of each peak. Fig. 6 depicts H_2-TPR profiles of CeO_2, 0.05Cu/CeO_2, 0.10Cu/CeO_2, 0.15Cu/CeO_2 and 0.20Cu/CeO_2 nanorods. Pure CeO_2 nanorods (Fig. 6a) show two broad peaks located at 411.9 °C and 709.6 °C, which are ascribed to the reduction of surface oxygen and bulk oxygen of CeO_2 [33, 34].

As shown in Fig. 6, doping Cu into CeO_2 results in significant modifications in the H_2-TPR profiles. All Cu/CeO_2 nanorods exhibit three reduction peaks, the first two peaks centered at temperature range of 130–142 °C (denoted as α) and 152–171 °C (denoted as β) are assigned to the reduction of finely dispersion copper oxide clusters interacting with the support of ceria and larger CuO particles non-associated with ceria [35]. The last peak located at ~ 721 °C is ascribed to the reduction of $Ce^{4+} \rightarrow Ce^{3+}$ [36]. It is obvious that the reduction peaks of Cu/CeO_2 nanorods shift to much lower temperatures compared to pure CeO_2 nanorods. What's more, with the increase of Cu doping, the reduction temperature of all Cu/CeO_2 nanorods (Table 3) is as the following trend: 0.15Cu/CeO_2 < 0.10Cu/CeO_2 < 0.05Cu/CeO_2 < 0.20Cu/CeO_2 < CeO_2, corresponding to the reduction ability of all nanorods follows the reverse trend: 0.15Cu/CeO_2 > 0.10Cu/CeO_2 > 0.05Cu/CeO_2 > 0.20Cu/CeO_2 > CeO_2, which is greatly agree with the XPS results and their CO catalytic activity.

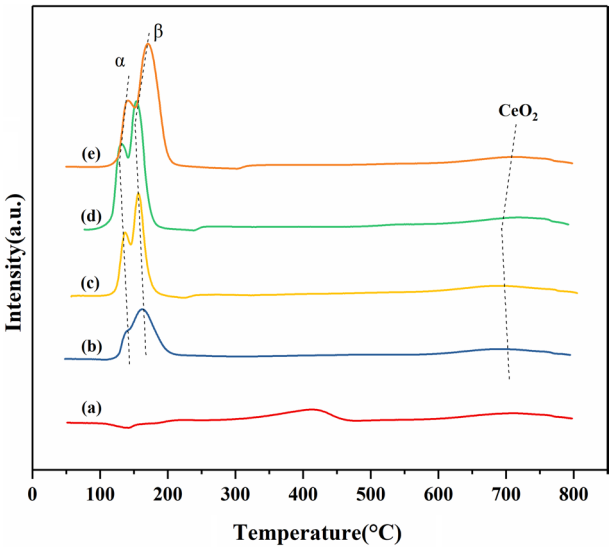

Fig. 6 H_2-TPR profiles of the obtained CeO_2 and Cu/CeO_2 nanorods: (a) CeO_2, (b) 0.05Cu/CeO_2, (c) 0.10Cu/CeO_2, (d) 0.15Cu/CeO_2, (e) 0.20Cu/CeO_2

Table 3 H_2 consumption amount and reduction temperature of Cu/CeO_2 samples

Sample	H_2 consumption (mmol/g)				Temperature (°C)	
	Peak α	Peak β	CeO_2 peak	Total	Peak α	Peak β
$0.05Cu/CeO_2$	0.286	0.666	0.707	1.659	139.4	162.1
$0.10Cu/CeO_2$	0.337	0.820	0.304	1.461	136.9	156.1
$0.15Cu/CeO_2$	0.538	1.209	0.388	2.135	130.6	152.3
$0.20Cu/CeO_2$	0.389	1.616	0.306	2.311	141.6	170.8

H_2 consumption of peak α, peak β and CeO_2 peak of the Cu/CeO_2 nanorods were also listed (Table 3). H_2 consumption at α peak increased with the increase of Cu/(Cu + Ce) atomic ratios from 0.05 to 0.15. H_2 consumption at α peak (0.389 mmol/g) of the $0.20Cu/CeO_2$ nanorods was lower than that (0.538 mmol/g) of the $0.15Cu/CeO_2$ nanorods, which was due to the presence of more CuO particles covered up CeO_2 surface [12]. The XRD (Fig. 5) could also prove that there were more bulk CuO on the surface of $0.20Cu/CeO_2$ samples. The results of H_2 consumption at α peak indicate that $0.15Cu/CeO_2$ nanorods perform the highest reducibility which could improve CO catalytic activity greatly.

CO-TPD

CO-TPD was used to obtain information on the CO adsorption and CO_2 desorption ability of the samples. The CO-TPD spectra of $0.15Cu/CeO_2$ and pure CeO_2 nanorods are displayed in Fig. 7. Desorption of CO_2 during the heating progress is observed for

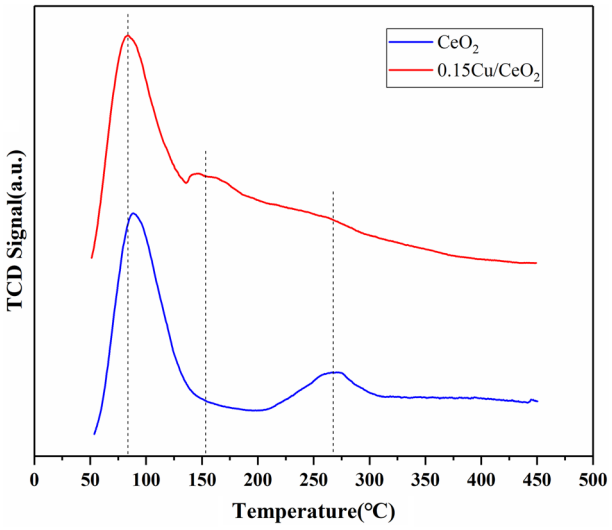

Fig. 7 CO-TPD profiles of $0.15Cu/CeO_2$ and CeO_2 nanorods

the two samples, indicating that the absorbed CO is completely oxidized into CO_2 by lattice oxygen in the samples. Obviously, three main peaks are observed for the 0.15Cu/CeO_2 nanorods while only two peaks are observed for pure CeO_2 nanorods. The peak around 85 °C may be corresponded to desorption of CO_2 which resulted from the reaction between adsorbed CO and surface oxygen. The peak at higher temperature (~267 °C) can be attributed to lattice oxygen which oxidizes CO to CO_2 [37]. As shown in Fig. 7, the introduction of Cu to CeO_2 nanorods leaded to a shift to a lower temperature of CO_2 desorption peak (~85 °C) by 7 °C, implying that the surface lattice oxygen and produced carbonate species of 0.15Cu/CeO_2 nanorods can be reduced and desorb more easily compared with pure CeO_2 nanorods. Moreover, the extra peak of 0.15Cu/CeO_2 nanorods at 154 °C, indicating that there are more active sites on the surface for CO adsorption [38]. The results of CO-TPD indicated that the addition of Cu to CeO_2 nanorods could increase the amount of active sites and make CO absorb on the active sites more easily, which was an important factor to improve the catalytic efficiency.

Conclusions

In summary, CeO_2 nanorods have smaller size and larger specific surface areas than other morphological characterization of CeO_2. 3D flower-like 0.10Cu/CeO_2, gear-like 0.10Cu/CeO_2 and xCu/CeO_2 nanorods (X = 0.05, 0.10, 0.15, 0.20) were synthesized by hydrothermal method and wet impregnation method for low temperature CO oxidation. The experimental results show that nanorod-like 0.10Cu/CeO_2 performs the best catalytic activity than 3D flower-like 0.10Cu/CeO_2 and gear-like 0.10Cu/CeO_2, the addition of copper can greatly improve the catalytic efficiency of CO, 0.15Cu/CeO_2 nanorods perform the best catalytic activity with a 99% CO conversion at 100 °C. The characterization by various instruments indicates 0.15Cu/CeO_2 nanorods have smaller crystallite sizes, higher relative ratio of Ce^{3+}, more oxygen vacancies, higher dispersion of Cu species together with more Cu^+ species, which should be responsible for the highest CO conversion at low temperature. Moreover, we have also investigated the influence of water vapor and CO_2 on the catalytic activity of 0.15Cu/CeO_2 nanorods. It is found that the catalyst has better resistance to CO_2 but worse resistance to water vapor.

Acknowledgements This work was supported by the National Key R&D Program of China (2019XKQYMS70), and Program for Changjiang Scholars and Innovative Research Team in University (IRT17R103).

Funding Funding was provided by the National Key R&D Program of China (2019XKQYMS70) and Science and Technology Innovative Research Team in Higher Educational Institutions of Hunan Province (CN) (IRT17R103).

References

1. Ebenstein A, Fan M, Greenstone M, He G, Zhou M (2017) New evidence on the impact of sustained exposure to air pollution on life expectancy from China's Huai River Policy. Proc Natl Acad Sci 114:10384–10389

2. Sandilands EA, Bateman DN (2016) Carbon monoxide. Medicine 44:151–152
3. Guo M, Lu J, Wu Y, Wang Y, Luo M (2011) UV and visible Raman studies of oxygen vacancies in rare-earth-doped ceria. Langmuir 27:3872–3877
4. Zhang J, Yang H, Wang S, Liu W, Liu X, Guo J, Yang Y (2014) Mesoporous CeO_2 nanoparticle sassembled by hollow nanostructures: formation mechanism and enhanced catalytic properties. Cryst Eng Comm 16:8777–8785
5. Haruta M, Yamada N, Kobayashi T, Iijima S (1989) Gold catalysts prepared by coprecipitation for low-temperature oxidation of hydrogen and of carbon monoxide. J Catal 115:301–309
6. Newton MA, Ferri D, Smolentsev G, Marchionni V, Nachtegaal M (2016) Room-temperature oxidation of carbon monoxide by oxygen over Pt/Al_2O_3 using combined, time-resolved XAFS, DRIFTS, and mass spectrometry. J Am Chem Soc 138:13930–13940
7. Campbell CT, Peden CHF (2005) Oxygen vacancies and catalysis on ceria surfaces. Science 309:713–714
8. Li Z, Han F, Li C, Jiao X, Chen D (2016) Hollow CeO_2 dodecahedrons: one-step template synthesis and enhanced catalytic performance. RSC Adv 6:60975–60982
9. Qu Z, Yu F, Zhang X, Wang Y, Gao J (2013) Support effects on the structure and catalytic activity of mesoporous Ag/CeO_2 catalysts for CO oxidation. Chem Eng J 229:522–532
10. Bao H, Zhang Z, Hua Q, Huang W (2014) Compositions, structures, and catalytic activities of $CeO_2@Cu_2O$ nanocomposites prepared by the template-assisted method. Langmuir 30:6427–6436
11. Zou W, Ge C, Lu M, Wu S, Wang Y, Sun J, Pu Y, Tang C, Gao F, Dong L (2015) Engineering the NiO/CeO_2 interface to enhance the catalytic performance for CO oxidation. RSC Adv 5:98335–98343
12. Hossain ST, Azeeva E, Zhang K, Zell ET, Bernard DT, Balaz S, Wang R (2018) A comparative study of CO oxidation over Cu-O-Ce solid solution and CuO/CeO_2 nanorods catalysts. Appl Surf Sci 455:132–143
13. Lykaki M, Pachatouridou E, Carabineiro SAC, Iliopoulou E, Andriopoulou C, Kallithrakas-Kontos N, Boghosian S, Konsolakis M (2018) Ceria nanoparticles shape effects on the structural defects and surface chemistry: implications in CO oxidation by Cu/CeO_2 catalysts. Appl Catal B 230:18–28
14. Jampaiah D, Venkataswamy P, Coyle VE, Reddy BM, Bhargava SK (2016) Low-temperature CO oxidation over manganese, cobalt, and nickel doped CeO_2 nanorods. RSC Adv 6:80541–80548
15. Chen XY, Wu CL, Guo ZZ (2019) Synthesis of efficient $Cu/CoFe_2O_4$ catalysts for low temperature CO oxidation. Catal Lett 149:399–409
16. Si R, Flytzani-Stephanopoulos M (2008) Shape and crystal-plane effects of nanoscale ceria on the activity of $Au-CeO_2$ catalysts for the water-gas shift reaction. Angew Chem Int Ed 47:2884
17. Zhong LS, Hu JS, Cao AM, Liu Q, Song WG, Wan LJ (2007) 3D flowerlike ceria micro/nanocomposite structure and its application for water treatment and CO removal. Chem Mater 19:1648–1655
18. Zhang C, Meng F, Wang L, Zhang M, Ding Z (2014) Morphology-selective synthesis method of gear-like CeO_2 microstructures and their optical properties. Mater Lett 130:202–205
19. Trovarelli A (1996) Catalytic properties of ceria and CeO_2-containing materials. Catal Rev Sci Eng 38:439–520
20. Gong X, Liu B, Kang B, Xu G, Wang Q, Jia C, Zhang J (2017) Microwave enhanced catalytic degradation of methyl orange in aqueous solution over CuO/CeO_2 catalyst in the absence and presence of H_2O_2. Mol Catal 436:90–99
21. Alla SK, Kollu P, Mandal RK, Prasad NK (2018) Formation of uniform CuO nanorods by spontaneous aggregation: selective synthesis of CuO, Cu_2O and Cu nanoparticles by a solid-liquid phase arc discharge process. Ceram Int 44:7221–7227
22. Xu D, Cheng F, Lu Q, Dai P (2014) Nanoshaped CuO/CeO_2 materials: effect of the exposed ceria surfaces on catalytic activity in N_2O decomposition reaction. Ind Eng Chem Res 53:2625–2632
23. Yao WT, Yu SH, Zhou Y, Jiang J, Wu QS, Zhang L, Jiang J (2005) Boosting Cu-Ce interaction in Cu_xO/CeO_2 nanocube catalysts for enhanced catalytic performance of preferential oxidation of CO in H_2-rich gases. J Phys Chem B 109:14011–14016
24. Zabilskiy M, Djinović P, Tchernychova E, Tkachenko OP, Kustov LM, Pintar A (2015) Magnetic properties of Cu doped CeO_2 nanostructures prepared by microwave refluxing technique. ACS Catal 5:5357–5365
25. Carabineiro SAC, Silva AMT, Dražić G, Tavares PB, Figueiredo JL (2010) Gold nanoparticles on ceria supports for the oxidation of carbon monoxide. Catal Today 154:21–30

26. Wang J, Zhong L, Lu J, Chen R, Lei Y, Chen K, Han C, He S, Wan G, Luo Y (2017) A solvent-free method to rapidly synthesize CuO-CeO_2 catalysts to enhance their CO preferential oxidation: effects of Cu loading and calcination temperature. Mol Catal 443:241–252
27. Liotta LF, Carlo DG, Pantaleo G, Venezia AM (2006) Co_3O_4/CeO_2 composite oxides for methane emissions abatement: relationship between Co_3O_4-CeO_2 interaction and catalytic activity. Appl Catal B Environ 66:217–227
28. Moretti E, Storaro L, Talon A, Riello P, Molina AI (2015) 3-D flower like Ce-Zr-Cu mixed oxide systems in the CO preferential oxidation (CO-PROX): effect of catalyst composition. Appl Catal B Environ 168–169:385–395
29. Avgouropoulos G, Ioannides T (2006) Effect of synthesis parameters on catalytic properties of CuO-CeO_2. Appl Catal B Environ 67:1–11
30. Polster CS, Nair H, Baertsch CD (2009) Study of active sites and mechanism responsible for highly selective CO oxidation in H_2 rich atmospheres on a mixed Cu and Ce oxide catalyst. J Catal 266:308–319
31. Aranda A, Agouram S, López JM, Mastral AM, Sellick DR, Solsona B, Taylor SH, García T (2012) Oxygen defects: the key parameter controlling the activity and selectivity of mesoporous copper-doped ceria for the total oxidation of naphthalene. Appl Catal B Environ 127:77–88
32. Santos VP, Carabineiro SAC, Bakker JJW, Soares OSGP, Chen X, Pereira MFR, Órfão JJM, Figueiredo JL, Gascon J, Kapteijn F (2014) Stabilized gold on cerium-modified cryptomelane: highly active in low-temperature CO oxidation. J Catal 309:58–65
33. Luo JY, Meng M, Li X, Li XG, Zha YQ, Hu TD, Xie YN, Zhang J (2008) Mesoporous Co_3O_4-CeO_2 and Pd/Co_3O_4-CeO_2 catalysts: synthesis, characterization and mechanistic study of their catalytic properties for low-temperature CO oxidation. J Catal 254:310–324
34. Liu J, Zhao Z, Wang J, Xu C, Duan A, Jiang G, Yang Q (2008) The highly active catalysts of nanometric CeO_2-supported cobalt oxides for soot combustion. Appl Catal B Environ 84:185–195
35. Guo X, Zhou R (2016) A new insight into the morphology effect of ceria on CuO/CeO_2 catalysts for CO selective oxidation in hydrogen-rich gas. Catal Sci Technol 6:3862–3871
36. Aboukaïs A, Skaf M, Hany S, Cousin R, Aouad S, Labaki M, Abi-Aad E (2016) A comparative study of Cu, Ag and Au doped CeO_2 in the total oxidation of volatile organic compounds (VOCs). Mater Chem Phys 177:570–576
37. Saw ET, Oemar U, Tan XR, Du Y, Borgna A, Hidajat K, Kawi S (2014) Bimetallic Ni-Cu catalyst supported on CeO_2 for high temperature water-gas shift reaction: methane suppression via enhanced CO adsorption. J Catal 314:32–46
38. Shen W, Mao D, Luo Z, Yu J (2017) CO oxidation on mesoporous SBA-15 supported CuO-CeO_2 catalyst prepared by a surfactant assisted impregnation method. RSC Adv 7:27689